Absence of detectable current-induced magneto-optical Kerr effects in Pt, Ta, and W

Patricia Riego' , Saül Vélez, Juan M. Gomez-Perez, Jon Ander Arregi' , Luis E. Hueso, Fèlix Casanova, and Andreas Berger

Absence of detectable current-induced magneto-optical Kerr effects in Pt, Ta, and W

Patricia Riego,[1,2,a)] Saül Vélez,[1] Juan M. Gomez-Perez,[1] Jon Ander Arregi,[1,b)] Luis E. Hueso,[1,3] Fèlix Casanova,[1,3] and Andreas Berger[1]

[1]*CIC nanoGUNE, E-20018 Donostia-San Sebastian, Spain*
[2]*Departamento de Física de la Materia Condensada, Universidad del País Vasco, UPV/EHU, E-48080 Bilbao, Spain*
[3]*IKERBASQUE, Basque Foundation for Science, E-48013 Bilbao, Spain*

We explore the possibility to detect spin accumulation due to the spin Hall effect (SHE) by means of the magneto-optical Kerr effect (MOKE). For this purpose, we utilize the generalized magneto-optical ellipsometry (GME), which enables the disentanglement of different magnetization components contributing to the resulting MOKE signal, and perform measurements for three different materials: Pt, W, and Ta. Although we observe a current-induced effect in the light intensity in our polarization sensitive GME setup, it does not arise from a SHE-induced light polarization signal in any of the materials, but from a change in reflectivity due to heating effects. Based on the sensitivity achieved in our experiments, we conclude that state-of-the-art magneto-optical methods utilizing linear optics are not sufficiently sensitive to detect SHE-induced spin accumulation in these metals. *Published by AIP Publishing.* [http://dx.doi.org/10.1063/1.4966276]

The spin Hall effect[1–5] (SHE) is an efficient technique for the generation of spin currents, which is based on the fact that, upon the injection of a charge current j_c in a thin film material with high spin-orbit coupling (SOC), electrons with spin up or down orientation are preferentially scattered in opposite directions, giving rise to a spin current j_s perpendicular to j_c. This also creates a spin accumulation μ_S that exhibits inverse spin polarization σ_S at opposite interfaces of the material. The detection of the SHE in metals is most commonly performed electrically, using approaches such as lateral spin valves,[6–10] spin pumping[11–13] or spin-torque ferromagnetic resonance.[14–16] Alternatively, one can detect the μ_S arising from the SHE by optical means, although until very recently this approach was limited to semiconductors.[17–21] Nevertheless, recent works have reported the possibility to detect μ_S in nonmagnetic metals optically, either induced by the contact with a ferromagnet[22] (FM) or originated by the SHE.[23–25] In particular, Ref. 23, which exploited the magneto-optical Kerr effect (MOKE), reported for a β-W sample a SHE-induced Kerr angle θ_K that is only five times smaller than that of a magnetically saturated Fe reference film. Thus, SHE-induced MOKE signals seem to open a new pathway for efficient SHE detection in metals.

In this work, we perform a detailed study on the possibility and limitations to detect SHE-induced μ_S in Pt, Ta, and W metals by magneto-optical (MO) means. For this purpose, we utilize generalized magneto-optical ellipsometry[26–28] (GME), a MOKE-based method that can separate pure optical reflectivity from MO signals, and allows one to determine the orientation of σ_S. Using this refined approach, we have found that the current-induced signals we observe are not of MO origin, and thus not related to the SHE.

We sputter-deposited two Pt samples (15 nm and 100 nm thick), a 15-nm-thick β-Ta sample, and a 15-nm-thick β-W sample onto low-doping Si/SiO$_2$(150 nm) substrates utilizing a Hall-bar-shaped shadow mask with a length of 6 mm and a width of 1 mm. X-ray reflectivity measurements were performed to control the thickness of the films, and resistivity and X-ray diffraction measurements to confirm that the desired β phase was achieved for Ta[15,29] and W.[16,30] Our choice of materials is motivated by the large spin Hall angles reported previously,[9,14–16,31] making them good candidates to exhibit a measurable MOKE signal.

Our MO setup is schematically shown in Fig. 1. The geometry is devised so that, upon the injection of an electrical current $\Im_{DC}$ along the long Hall bar channel (x-axis), the SHE leads to a σ_S oriented along the y-axis (see Fig. 1), giving rise to the longitudinal (L-) MOKE. The voltage drop in the sample is measured simultaneously in order to monitor the sample resistance. The optical setup is rather simple, consisting of a continuous wave (CW) low-noise laser, which emits intensity and polarization stabilized light at wavelength $\lambda = 635$ nm. The light beam first passes through a linear polarizer P_1 mounted on a rotation stage, is then reflected by the central part of the Hall bar structure, and subsequently passes through a second rotatable polarizer P_2. The light intensity I after P_2 is detected by a photodiode, which includes a filter so that the ambient light is blocked. The light beam itself is not modulated in our experiments. The described setup is polarization-sensitive, in that the detected I will change if the reflected light acquires a polarization change due to the MOKE associated with σ_S at the sample surface. Hereby, the normalized change in I upon inversion of σ_S, i.e., upon inversion of the applied current,[2] is given by

$$\frac{\delta I}{I} = 2\frac{I(+\boldsymbol{\sigma}_S) - I(-\boldsymbol{\sigma}_S)}{I(+\boldsymbol{\sigma}_S) + I(-\boldsymbol{\sigma}_S)} = 2\frac{I(+\Im_{DC}) - I(-\Im_{DC})}{I(+\Im_{DC}) + I(-\Im_{DC})}. \quad (1)$$

a)E-mail: p.riego@nanogune.eu
b)Present address: CEITEC Brno University of Technology, Purkyňova 123, 612 00 Brno, Czech Republic.
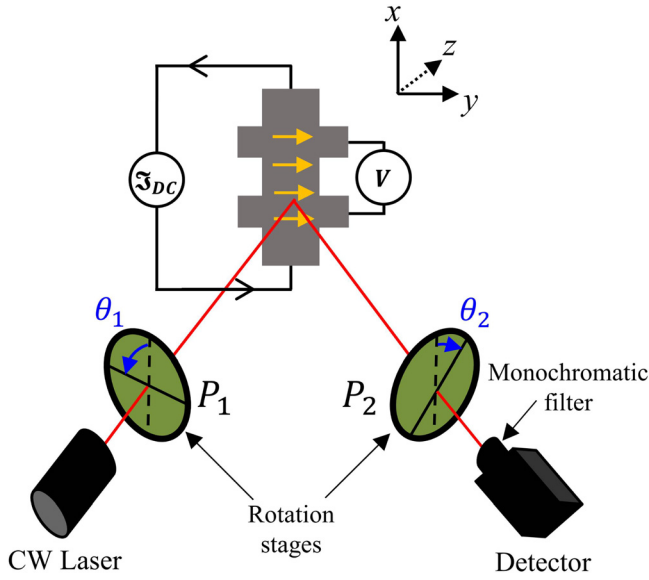
FIG. 1. Schematics of the measurement setup. A CW laser illuminates the central part of the Hall bar at a 45° angle of incidence. Two polarizers P_1 and P_2 mounted on rotation stages are rotated by angles θ_1 and θ_2, respectively. The light intensity after P_2 is detected by a photodiode detector. A current source drives a current $\Im_{DC}$ along the long channel of the Hall bar, while a voltmeter measures the generated voltage drop V. The horizontal arrows in the sample represent the expected SHE-induced $\boldsymbol{\sigma}_S$ in our experiment.

FIG. 2. Symmetry properties of $\delta I/I\,(\theta_1,\theta_2)$ maps representing MOKE-signals for different magnetization orientations (corresponding scale bars are shown on the right hand side in each figure): (a) Longitudinal, (b) transverse, and (c) combination of longitudinal and transverse.

In conventional MOKE experiments, the orientations of P_1 and P_2 are fixed, typically near the crossed polarizers configuration, for which $\delta I/I$ is proportional to the Kerr rotation[32] θ_K. This MOKE detection scheme, however, can access only partial information and mixes various MO and purely optical contributions.[32–35] The maximum information that one can retrieve from a reflection experiment is the reflection matrix, which for our samples exhibiting in-plane $\boldsymbol{\sigma}_S$ is[26,28]

$$\boldsymbol{R} = \begin{pmatrix} r_s & \alpha \\ -\alpha & r_p + \beta \end{pmatrix} = r_p \begin{pmatrix} \tilde{r}_s & \tilde{\alpha} \\ -\tilde{\alpha} & 1 + \tilde{\beta} \end{pmatrix}. \qquad (2)$$

Here, r_s and r_p are the non-magnetic Fresnel coefficients, $\tilde{\alpha}$ is related to L-MOKE, i.e., the spin component along y, and $\tilde{\beta}$ to the transverse (T-) MOKE, i.e., the spin component along x. Thus, the determination of $\boldsymbol{R}$ enables the separation of optical and MO contributions as well as the disentanglement of the different components of $\boldsymbol{\sigma}_S$. GME now achieves the determination of $\boldsymbol{R}$ by performing $\delta I/I$ measurements [Eq. (1)] for different combinations of angles θ_1 and θ_2 as indicated in Fig. 1. For a sample described by the reflection matrix in Eq. (2), $\delta I/I$ can be written as

$$\frac{\delta I}{I}(\theta_1,\theta_2) = 4\frac{B_1 f_1 + B_2 f_2 + B_3 f_3 + B_4 f_4}{f_3 + B_5 f_5 + 2B_6 f_4}, \qquad (3)$$

where the B_i factors are functions of the elements in $\boldsymbol{R}$, and $f_i = f_i(\theta_1,\theta_2)$ are analytical functions of θ_1 and θ_2 (Refs. 26 and 28). By measuring $\delta I/I$ for various (θ_1, θ_2) angles and by fitting the data to Eq. (3), one can now determine the B_i parameters and thus the elements in $\boldsymbol{R}$.

Importantly, $\delta I/I\,(\theta_1,\theta_2)$ exhibits specific symmetries for different $\boldsymbol{\sigma}_S$ orientations. In the L-MOKE case with $\boldsymbol{\sigma}_S \parallel y$, shown in Fig. 2(a), $\delta I/I$ exhibits two lobes of

opposite sign that meet at the crossing point of the polarizers $\theta_1 = 90°$, $\theta_2 = 0°$. In the T-MOKE case, when $\boldsymbol{\sigma}_S \parallel x$, the lobes of $\delta I/I$ centered at the crossing point have the same sign, as can be seen in Fig. 2(b). When an in-plane $\boldsymbol{\sigma}_S$ is at an intermediate angle, the pattern is an additive combination of L- and T-MOKE, as shown in Fig. 2(c), and can be easily disentangled. Polar MOKE ($\boldsymbol{\sigma} \parallel z$), which is not considered in this work, can also be unambiguously determined in GME because of its own distinct symmetry properties with respect to θ_1 and θ_2.

We have performed GME measurements in our samples by alternatively applying $+\Im_{DC}$ and $-\Im_{DC}$ currents, and by measuring the photodetector signal for different (θ_1, θ_2) configurations. The subsequently constructed $\delta I/I\,(\theta_1,\theta_2)$ maps are shown in Figs. 3(a)–3(d), and none of them displays the MOKE signal symmetries discussed in conjunction with Fig. 2, let alone the specific L-MOKE symmetry of Fig. 2(a) expected for our experiment. Instead, we find a distribution of non-vanishing $\delta I/I$ values appearing randomly near the diagonal of the maps. This "noise diagonal" arises because here the difference between θ_1 and θ_2 is close to $90°$ and thus I is very low, making $\delta I/I\,(\theta_1,\theta_2)$ rather noisy.[28] The here-observed noise level is not unexpectedly large, but corresponds to the typical noise floor for any GME measurement,[27] so that our results clearly indicate the absence of a measureable MO effect.

We have quantified the signals by fitting the $\delta I/I$ data of each sample to Eq. (3). The fittings are shown in Figs. 3(e)–3(h) in the same color scale as the experimental data, and hardly any actual signal pattern can be extracted *via* the
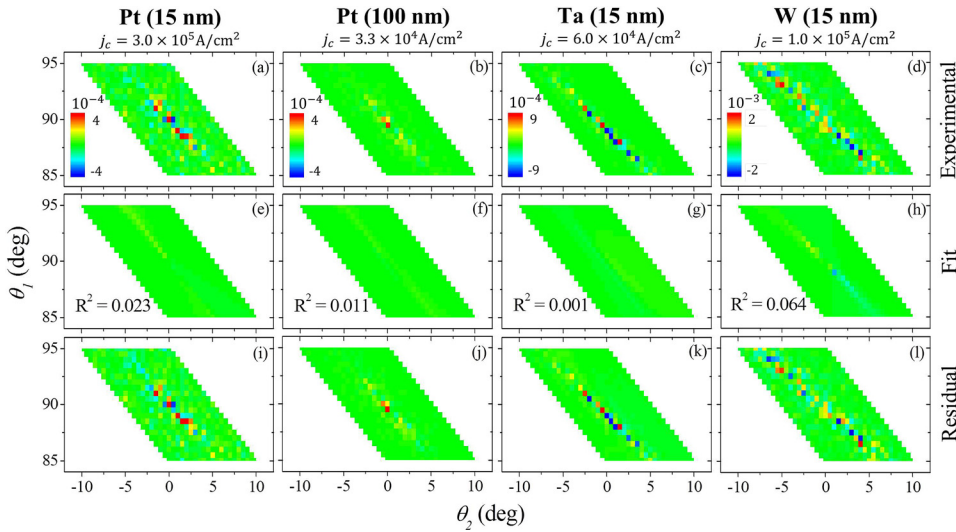
FIG. 3. (a)–(d) Experimental $\delta I / I(\theta_1, \theta_2)$ maps for the four samples; (e)–(h) Least-squares fits of the measured maps to Eq. (3). The insets show the R^2 goodness values of the fits. (i)–(l) Difference between experimental data and fits. Each column corresponds to the sample and the current density value specified on top. The scale bars for the maps corresponding to each sample are displayed inside (a)–(d), respectively.

fits. The R^2 goodness values of the fits, which are shown in Figs. 3(e)–3(h), are very low, because the symmetries of the fit function are not present in the data. In addition, residual maps displaying the difference between the measurements and fits shown in Figs. 3(i)–3(l) are almost identical to the measurements, corroborating that the measured data cannot be explained as a MOKE-induced light polarization effect. In contrast, for samples that exhibit a sufficiently large MOKE signal, GME maps show clear symmetry patterns, and least-squares fits to Eq. (3) yield R^2 values of 0.99 or better.[26–28,36,37]

Our comprehensive data analysis now allows us to determine the upper bounds for the MOKE signal. Specifically, we have determined θ_K values, which are listed in Table I with error bars corresponding to a 95% confidence interval. For all samples, the size of the error bar is comparable to the mean value of θ_K, indicating that the contribution of L-MOKE to our experimental data is negligible, despite achieving a detection limit of better than 10^{-7} rad (i.e., below 0.05 mdeg) in all cases. Table I also shows the measured θ_K values normalized to the applied current density j_C. Our data are in obvious disagreement with the findings of Ref. 23, where the reported θ_K / j_C values are two orders of magnitude larger than the detection limit we achieved here using GME, so that we should have been able to detect them, if they were indeed present.

A possible explanation for the inconsistency of our experimental results with prior reports is the difference between conventional MOKE and the GME methodology. In conventional MOKE, the determination of θ_K relies on a net intensity change in a polarization sensitive experiment, such as using a single (θ_1, θ_2)-configuration for the setup in Fig. 1. However,

such experimental conditions can be susceptible to false positives if the experiment generates a light intensity change that is unrelated to an actual polarization effect. This can generate particularly high $\delta I / I$ values if one operates at low intensity levels, as demonstrated by the "noise diagonal" in our maps. The strength of GME is that by acquiring $\delta I / I$ for several (θ_1, θ_2) configurations, it allows for the separation of actual MOKE effects from such spurious signals, because the MOKE signal has to fulfill the symmetries described by Eq. (3).

We performed additional measurements to investigate the origin of the spurious signal-like noise features at certain polarizer conditions. It is known that (i) the SHE-induced μ_S is proportional to the applied current,[2] (ii) the expected $\boldsymbol{\sigma}_S \parallel y$ gives rise to a θ_K that is proportional to μ_S (Ref. 32), and (iii) near the crossed-polarizer configuration, the detected light intensity depends linearly on θ_K (Ref. 32). Altogether, if a signal is SHE-related, the light intensity should be linear in $\Im_{DC}$ near the crossed-polarizer configuration. To test this, we fixed P_1 and P_2 close to being crossed ($\theta_1 = 90°$, $\theta_2 = 5°$) and measured the photodetector signal as $\Im_{DC}$ is swept. The result, shown in Fig. 4(a) for the Pt (15 nm) sample, does not show a linear trend, but rather a slightly hysteretic, quadratic light intensity dependence on $\Im_{DC}$, which is not MOKE-related. This is the case because, even if our setup is devised to be polarization-sensitive, it also senses non-polarization induced absolute changes in sample reflectivity. Correspondingly, the signal in Fig. 4(a) can be explained by a change of the sample reflectivity due to heating effects, which are proportional to $\Im_{DC}^2$. The simultaneously monitored four-point resistance, shown in Fig. 4(b), also exhibits a slightly hysteretic quadratic dependence on $\Im_{DC}$ consistent with Joule heating. The same kind of experiment was performed without polarizer P_2, thus

TABLE I. Columns 1–3: Sample material and thickness, resistivity, and applied current amplitude during the GME experiment. Column 4: θ_K obtained from the GME data analysis. Column 5: θ_K normalized to the applied current density.

Sample	ρ ($\mu\Omega \times$ cm)	$\Im_{DC}$ (mA)	θ_K (mdeg)	θ_K / j_c (deg $\times$ (A/cm^2)$^{-1}$)
Pt (15 nm)	31	45	$(-0.88 \pm 3.22) \times 10^{-3}$	$(-0.29 \pm 1.07) \times 10^{-11}$
Pt (100 nm)	25	33	$(2.19 \pm 1.36) \times 10^{-3}$	$(6.64 \pm 4.12) \times 10^{-11}$
β-Ta (15 nm)	180	9	$(1.78 \pm 4.56) \times 10^{-2}$	$(2.97 \pm 7.60) \times 10^{-10}$
β-W (15 nm)	225	15	$(-1.03 \pm 1.19) \times 10^{-2}$	$(-1.03 \pm 1.19) \times 10^{-10}$
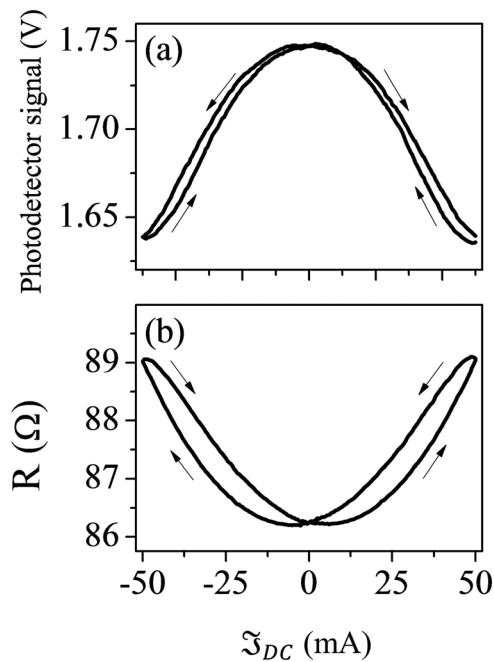
FIG. 4. Simultaneously measured (a) photodetector signal and (b) resistance as a function of the applied current, for the 15 nm Pt sample and polarizer orientations of $\theta_1 = 90°$ and $\theta_2 = 5°$.

removing the polarization sensitivity from our setup, and results equivalent to those in Fig. 4(a) were obtained. Ta and W samples also show a quadratic $I(\Im_{DC})$ dependence. Under ideal measurement conditions, this quadratic dependence would give rise to a null $\delta I = I(+\Im_{DC}) - I(-\Im_{DC})$ signal. However, due to the hysteretic behavior, noise sources, and other experimental imperfections, the light intensity upon current inversion might not be completely identical, thus causing non-zero δI values. This is the key reason for the scattered nonzero $\delta I/I$ values in our GME maps, especially near the (θ_1, θ_2)-plane diagonal.

The inability to detect a SHE-induced MOKE in Pt, Ta, and W metals with our state-of-the-art linear MOKE experiment can be explained *via* a simple physical picture. For the here-utilized current density values, the electrons that participate in the transport and that can be potentially polarized *via* the SHE constitute a very small fraction of the conduction band electrons. However, the number of electrons that participate in optical reflection for these metals and photon energies of 2 eV is vastly larger. Therefore, the ratio between spin-polarized electrons and probed ones is many orders of magnitude smaller here than in MOKE experiments on ferromagnets. We estimate expected θ_K values to be up to 5 orders of magnitude below our 10^{-2} mdeg detection limit. The situation is different in semiconductors,[17–21] as well as in the case of other techniques, because the ratio between spin-polarized electrons and signal generating ones can be vastly larger.[24,25] Also, one can resort to MOKE techniques to probe SHE-induced effects rather than attempt the direct detection of SHE-generated spin accumulation. For instance, in heavy metal/ferromagnet bilayers, recent works have shown that MOKE is well suited to detect changes in magnetization in the ferromagnetic layer that occur due to spin torques that originate from the SHE in the heavy metal layer.[38–40]

In conclusion, our measurements demonstrate that potential MOKE signals arising from the SHE in Pt, Ta, and W are all below the detection limits of our state-of-the-art setup despite our excellent Kerr rotation sensitivity of 0.05 mdeg. However, we observe current-induced reflectivity effects that are quadratic in $\Im_{DC}$, which are caused by sample heating, as evidenced by simultaneously occurring resistivity changes. Such non-SHE-related effects generate a certain level of noise and can lead to spurious signals in polarization-sensitive detection experiments under low light intensity conditions. By performing complete GME-type measurements, we are able to unambiguously distinguish such purely optical effects from actual MOKE polarization signals.

[1]M. I. Dyakonov and V. I. Perel, Phys. Lett. **A 35**, 459 (1971).
[2]J. E. Hirsch, Phys. Rev. Lett. **83**, 1834 (1999).
[3]S. Maekawa, S. O. Valenzuela, E. Saitoh, and T. Kimura, *Spin Currents* (Oxford University Press, New York, 2012).
[4]A. Hoffmann, IEEE Trans. Magn. **49**, 5172 (2013).
[5]J. Sinova, S. O. Valenzuela, J. Wunderlich, C. H. Back, and T. Jungwirth, Rev. Mod. Phys. **87**, 1213 (2015).
[6]S. O. Valenzuela and M. Tinkham, Nature **442**, 176 (2006).
[7]T. Kimura, Y. Otani, T. Sato, S. Takahashi, and S. Maekawa, Phys. Rev. Lett **98**, 156601 (2007).
[8]P. Laczkowski, J.-C. Rojas-Sánchez, W. Savero-Torres, H. Jaffrès, N. Reyren, C. Deranlot, L. Notin, C. Beigné, A. Marty, J.-P. Attané, L. Vila, J.-M. George, and A. Fert, Appl. Phys. Lett. **104**, 142403 (2014).
[9]E. Sagasta, Y. Omori, M. Isasa, M. Gradhand, L. E. Hueso, Y. Niimi, Y. Otani, and F. Casanova, Phys. Rev. B **94**, 060412(R) (2016).
[10]M. Isasa, E. Villamor, L. E. Hueso, M. Gradhand, and F. Casanova, Phys. Rev. B **91**, 024402 (2015); **92**, 019905(E) (2015).
[11]E. Saitoh, M. Ueda, H. Miyajima, and G. Tatara, Appl. Phys. Lett. **88**, 182509 (2006).
[12]K. Ando, S. Takahashi, K. Harii, K. Sasage, J. Ieda, S. Maekawa, and E. Saitoh, Phys. Rev. Lett. **101**, 036601 (2008).
[13]Y. Kajiwara, K. Harii, S. Takahashi, J. Ohe, K. Uchida, M. Mizuguchi, H. Umezawa, H. Kawai, K. Ando, K. Takanashi, S. Maekawa, and E. Saitoh, Nature **464**, 262 (2010).
[14]L. Liu, T. Moriyama, D. C. Ralph, and R. A. Buhrman, Phys. Rev. Lett. **106**, 036601 (2011).
[15]L. Liu, C. F. Pai, Y. Li, H. W. Tseng, D. C. Ralph, and R. A. Buhrman, Science **336**, 555 (2012).
[16]C.-F. Pai, L. Liu, Y. Li, H. W. Tseng, D. C. Ralph, and R. A. Buhrman, Appl. Phys. Lett. **101**, 122404 (2012).
[17]Y. K. Kato, R. C. Myers, A. C. Gossard, and D. D. Awschalom, Science **306**, 1910 (2004).
[18]V. Sih, R. C. Myers, Y. K. Kato, W. H. Lau, A. C. Gossard, and D. D. Awschalom, Nat. Phys. **1**(1), 31 (2005).
[19]J. Wunderlich, B. Kaestner, J. Sinova, and T. Jungwirth, Phys. Rev. Lett. **94**, 047204 (2005).
[20]S. A. Crooker, M. Furis, X. Lou, C. Adelmann, D. L. Smith, C. J. Palmstrøm, and P. A. Crowell, Science **309**, 2191 (2005).
[21]N. P. Stern, D. W. Steuerman, S. Mack, A. C. Gossard, and D. D. Awschalom, Appl. Phys. Lett. **91**, 062109 (2007).
[22]R. Kukreja, S. Bonetti, Z. Chen, D. Backes, Y. Acremann, J. A. Katine, A. D. Kent, H. A. Dürr, H. Ohldag, and J. Stöhr, Phys. Rev. Lett. **115**, 096601 (2015).
[23]O. M. J. van't Erve, A. T. Hanbicki, K. M. McCreary, C. H. Li, and B. T. Jonker, Appl. Phys. Lett. **104**, 172402 (2014).

[24]A. Pattabi, Z. Gu, J. Gorchon, Y. Yang, J. Finley, O. J. Lee, H. A. Raziq, S. Salahuddin, and J. Bokor, Appl. Phys. Lett. **107**, 152404 (2015).

[25]H. J. Zhang, S. Yamamoto, Y. Fukaya, M. Maekawa, H. Li, A. Kawasuso, T. Seki, E. Saitoh, and K. Takanashi, Sci. Rep. **4**, 4844 (2014).

[26]A. Berger and M. R. Pufall, Appl. Phys. Lett. **71**, 965 (1997).

[27]A. Berger and M. R. Pufall, J. Appl. Phys. **85**, 4583 (1999).

[28]J. A. Arregi, J. B. Gonzalez-Diaz, E. Bergaretxe, O. Idigoras, T. Unsal, and A. Berger, J. Appl. Phys. **111**, 103912 (2012).

[29]M. H. Read and C. Altman, Appl. Phys. Lett. **7**, 51 (1965).

[30]Q. Hao, W. Chen, and G. Xiao, Appl. Phys. Lett. **106**, 182403 (2015).

[31]S. Vélez, V. N. Golovach, A. Bedoya-Pinto, M. Isasa, E. Sagasta, M. Abadia, C. Rogero, L. E. Hueso, F. S. Bergeret, and F. Casanova, Phys. Rev. Lett. **116**, 016603 (2016).

[32]Z. Q. Qiu and S. D. Bader, Rev. Sci. Instrum. **71**, 1243 (2000).

[33]E. R. Moog and S. D. Bader, Superlattices Microstruct. **1**, 543 (1985).

[34]Z. Q. Qiu, J. Pearson, A. Berger, and S. D. Bader, Phys. Rev. Lett. **68**, 1398 (1992).

[35]J. McCord, J. Phys. D: Appl. Phys. **48**, 333001 (2015).

[36]J. B. González-Díaz, J. A. Arregi, E. Bergaretxe, M. J. Fertin, O. Idigoras, and A. Berger, J. Magn. Magn. Mater. **325**, 147 (2013).

[37]J. A. Arregi, J. B. González-Díaz, O. Idigoras, and A. Berger, Phys. Rev. B **92**, 184405 (2015).

[38]X. Fan, H. Celik, J. Wu, C. Ni, K.-J. Lee, V. O. Lorenz, and J. Q. Xiao, Nat. Commun. **5**, 3042 (2014).

[39]M. Montazeri, P. Upadhyaya, M. C. Onbasli, G. Yu, K. L. Wong, M. Lang, Y. Fan, X. Li, P. K. Amiri, R. N. Schwartz, C. A. Ross, and K. L. Wang, Nat. Commun. **6**, 8958 (2015).

[40]X. Fan, A. R. Mellnik, W. Wang, N. Reynolds, T. Wang, H. Celik, V. O. Lorenz, D. C. Ralph, and J. Q. Xiao, Appl. Phys. Lett. **109**, 122406 (2016).